TRENDS IN SCIENCES 2025; 22(11): 10800
https://doi.org/10.48048/tis.2025.10800
RESEARCH ARTICLE

Exploration of Antituberculosis Potential of Ni(II) and Zn(II) Serine-Tyrosine Dithiocarbamate Complexes: Synthesis, Characterization, *In Silico* Profile, and *In Vitro* Evaluation

Wildan Mubaraq[1], Indah Raya[1,*], Herlina Rasyid[1], Nunuk Hariani Soekamto[1], Hasnah Natsir[1], Djabal Nur Basir[1], Rizal Irfandi[2], Bulkis Musa[1], Erna Mayasari[1], Wanda Wardyanti[1], Andi Adillah Nur Syafirah[4], Desy Kartina[3] and Santi Santi[5]

[1]*Department of Chemistry, Faculty of Mathematics and Natural Science, Hasanuddin University, Makassar 90245, Indonesia*
[2]*Department of Chemistry, Faculty of Mathematics and Natural Science, Universitas Negeri Makassar, Makassar 90244, Indonesia*
[3]*Departement of Chemistry, Pakuan University, Bogor-PO BOX 452, Indonesia*
[4]*Departement of Internal Medicine, Faculty of Medicine, Hasanuddin University, Makassar 90245, Indonesia*
[5]*Medical Laboratory Technology, Faculty of Health Technology, Megarezky University, Makassar 90234, Indonesia*

([*]Corresponding author's e-mail: indahraya@unhas.ac.id)

Received: 30 May 2025, Revised: 13 June 2025, Accepted: 25 June 2025, Published: 5 August 2025

Abstract

Tuberculosis (TB) remains a global health challenge, with millions of new cases and deaths reported each year. The emergence of drug resistance and treatment side effects has driven the development of new therapeutic agents, including the use of dithiocarbamate metal complex compounds. This study aims to synthesize and characterize Ni(II) and Zn(II) complexes with serine-tyrosine dithiocarbamate ligands and evaluate their antituberculosis bioactivity. The method in this study involves the synthesis and characterization of Ni(II) and Zn(II) complexes with serine-tyrosine dithiocarbamate, including melting point determination, conductivity measurement, and spectroscopic analyses (UV-Vis, FT-IR, XRD, and SEM-EDS). Furthermore, the bioactivity of the synthesized metal complexes was evaluated using both *in silico* approaches (Lipinski's rule of 5, ADMET profiling, and molecular docking) and *in vitro* testing using the Lowenstein-Jensen method. The synthesis and characterization results show that the successfully synthesized metal complexes are solid, non-electrolyte, stable, and have typical characteristics of dithiocarbamate complexes. *In silico* analysis shows compliance with Lipinski's rule and most ADMET parameters, indicating potential as oral drug candidates. Molecular docking revealed strong interactions, particularly for the Ni(II)Ser-Tyr Dtc complex with the highest binding score (−95.0923 kJ/mol), exceeding INH (−65.8232 kJ/mol). *In vitro* results confirmed antibacterial activity by the absence of *M. tuberculosis* H37Rv colony growth. These findings suggest the metal complexes have potential as antituberculosis agents.

Keywords: Metal-complexes, Peptide-dithiocarbamate, Antituberculosis, *M. tuberculosis*, Molecular docking

Introduction

Tuberculosis (TB), an infectious disease caused by *Mycobacterium tuberculosis*, remains a major global health concern. Approximately 10 million new TB cases and 1.5 million related deaths are reported annually worldwide [1,2]. The emergence of drug-resistant strains, such as MDR-TB (resistant to isoniazid and rifampicin) and XDR-TB (additionally resistant to fluoroquinolones and second-line injectable drugs like amikacin), has worsened TB control efforts. These resistant forms mainly arise from incomplete treatment,

poor drug quality, and patient non-adherence, which enable the bacteria to survive and develop resistance [3,4]. One promising approach is the utilization of metal complexes as antibacterial agents [5]. These compounds are believed to have a lower tendency to induce drug resistance due to their multi-target mechanisms of action, including disruption of microbial cell membranes, interaction with DNA or proteins, and generation of reactive oxygen species (ROS) [6-8]. This multifaceted mode of action makes it more difficult for bacteria to develop effective resistance, unlike conventional antibiotics that often target a single biomolecular pathway. Among various metal-based antibacterial agents, metal complexes containing dithiocarbamate ligands have demonstrated significant activity against pathogens such as *Staphylococcus aureus*, *Escherichia coli*, and *Candida albicans* [9,10]. Their antibacterial effect, particularly against *M. tuberculosis*, is mainly due to their capacity to chelate essential metal ions, inhibit key enzymes, and induce oxidative stress, thereby disrupting bacterial survival.

Dithiocarbamates are recognized as potent bidentate ligands capable of forming stable metal complexes with transition metals such as nickel and zinc, which can enhance their antimicrobial activity against bacteria [11-13]. Previous studies reported that Ni(II) and Zn(II) dithiocarbamate complexes exhibited significant antibacterial and antifungal activities. Zn(II) metal complexes showed strong antibacterial activity with inhibition zones of 26 - 29 mm, while Ni(II) metal complexes ranged from 14 - 23 mm against *Rhodococcus*, *E. coli, B. subtilis*, and *P. aeruginosa*. As for antifungal activity, Zn(II) metal complexes showed inhibition zones (19 - 28 mm) and Ni(II) metal complexes (18 - 23 mm) against *A. niger, A. flavus, C. albicans*, and *Acetomyceta* [14]. However, these studies primarily employed simple ligands without modification by biologically relevant amino acids. In this study, serine-tyrosine dipeptides were employed as ligands due to their polar side chains, which may improve solubility, membrane permeability, and interaction with biological targets. The hydroxyl group in tyrosine and the nucleophilic nature of serine enhance metal coordination, potentially improving the pharmacokinetic profile of the metal complexes [15-17]. The incorporation of serine-tyrosine dipeptides as ligands in Ni(II) and Zn(II) dithiocarbamate complexes for antitubercular applications remains unexplored, representing a novel approach to improving drug-like properties and antimicrobial efficacy against *M. tuberculosis*.

The incorporation of peptide ligands such as serine-tyrosine introduces additional functional groups capable of forming hydrogen bonds, strengthening metal coordination, and facilitating molecular recognition in biological systems. This may increase the binding affinity of the metal complexes toward key enzymatic targets of *M. tuberculosis*, such as enoyl-ACP reductase (InhA), a critical enzyme in TB drug development [18]. To verify this potential mechanism and validate the drug-likeness of the complexes, a comprehensive evaluation was undertaken. This study integrates synthesis, spectroscopic characterization, *in silico* evaluations (including molecular docking, Lipinski's rule of 5, and ADMET profiling), and *in vitro* testing against *M. tuberculosis* H37Rv to comprehensively evaluate the therapeutic potential of the complexes. This integrated strategy aims to identify novel dithiocarbamate-based metal complexes as promising antitubercular candidates.

Materials and methods

The materials used in this study included $NiCl_2 \cdot 6H_2O$ (Merck), $ZnCl_2$ (Merck), cysteine (Merck), serine (Merck), carbon disulfide (CS_2) (Merck), KOH, ethanol (Merck), 1% NaCl, dimethyl sulfoxide, (Merck), potassium bromide (KBr), Medium Lowenstein Jensen, and *Mycobacterium tuberculosis* H37Rv bacteria.

Preparation of serine-tyrosine ditiocarbamate ligands

Serine-tyrosine dithiocarbamate was synthesized using an *in situ* method. First, 0.2805 g (5 mmol) of KOH was dissolved in distilled water. Then, 0.302 mL (5 mmol) of CS_2 was added dropwise to the ice-cooled solution while stirring. Next, 0.906 g (5 mmol) of tyrosine, dissolved in 10 mL of ethanol, was added to the mixture, followed by the addition of 0.5254 g (5 mmol) of serine, also dissolved in 10 mL of ethanol. The reaction mixture was stirred vigorously for 30 min using a magnetic stirrer. The resulting precipitate was filtered, dried in a desiccator, and recrystallized with ethanol to obtain pure crystals. The synthesis reaction of tyrosine-

serine dipeptide dithiocarbamate is illustrated in **Figure 1**.

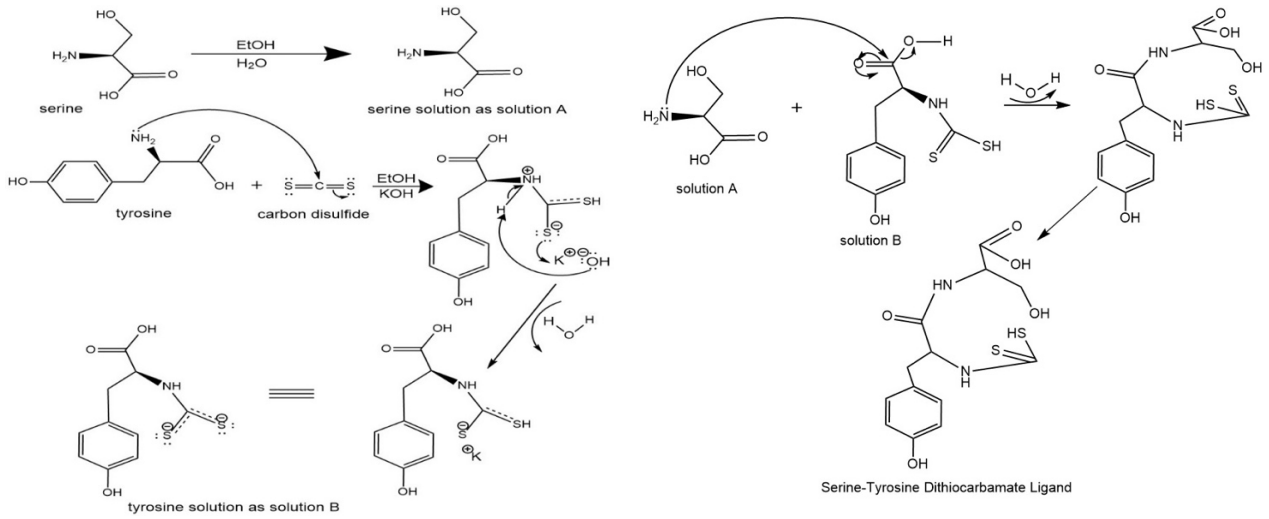

Figure 1 Synthesis reaction of serine-tyrosine dithiocarbamate ligands.

Synthesis of Ni(II) and Zn(II) with serine-tyrosine ditiocarbamate ligand

The Ni(II) complex was prepared by adding 10 mL of a 0.7130 g (3 mmol) $NiCl_2 \cdot 6H_2O$ ethanolic solution into 10 mL of a serine-tyrosine dithiocarbamate ligand solution (1:2 molar ratio) and stirring for 30 min. Similarly, the Zn(II) complex was synthesized by mixing 10 mL of a 0.4088 g (3 mmol) $ZnCl_2$ ethanolic solution with 10 mL of a serine-tyrosine dithiocarbamate ligand solution (1:2 molar ratio) and stirring for 30 min. The resulting precipitate was filtered, dried in a desiccator, and recrystallized with ethanol to obtain pure crystals. The synthesis reaction of Ni(II) and Zn(II) complexes with serine-tyrosine dithiocarbamate ligands is illustrated in **Figures 2** and **3**.

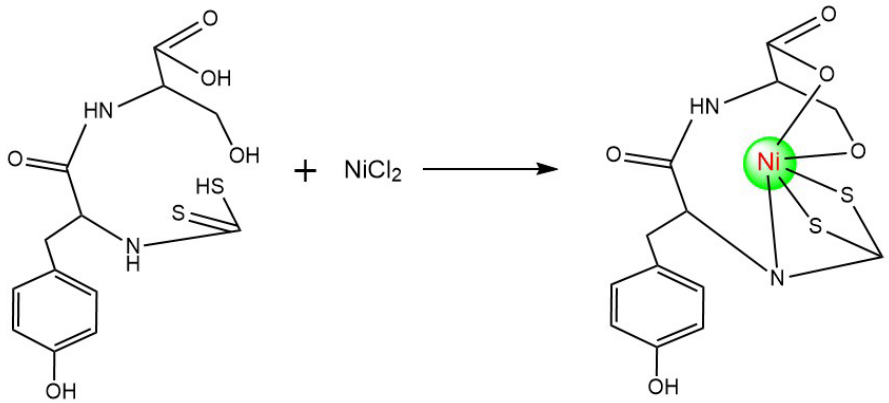

Figure 2 Synthesis reaction of Ni(II)serine-tyrosine dithiocarbamate complex.

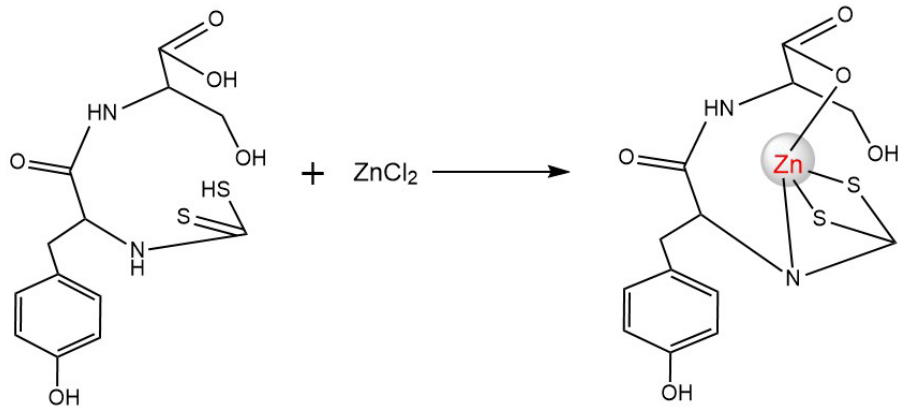

Figure 3 Synthesis reaction of Zn(II)serine-tyrosine dithiocarbamate complex.

Characterization of metal complexes

The metal complexes Ni(II)Ser-Tyr Dtc and Zn(II)Ser-Tyr Dtc were characterized based on their physicochemical properties. The metal complexes were dissolved in ethanol, and their electrical conductivities were measured using a Lutron CD-4303 conductometer. Subsequently, the metal complexes were placed into capillary tubes, and their melting points were determined using an Electrothermal IA 9100 melting point apparatus. The electronic spectra were then recorded using a Spectronic 20D+ UV-Visible spectrophotometer in the wavelength range of 200 - 800 nm. For FT-IR spectral analysis, the metal complexes were prepared as KBr pellets and analyzed with a Shimadzu Prestige-21 FT-IR spectrometer over a wavenumber range of 4000 - 340 cm^{-1}. The crystal structures were confirmed using a Shimadzu XRD-7000 Maxima-90° diffractometer with a step interval of 0.02° per step, generating diffractograms of diffraction angle (2θ) versus peak intensity. Furthermore, the morphology, particle size, and elemental composition of the metal complexes were examined using a JEOL JCM-300 Plus SEM-EDS instrument.

Analysis of Lipinski Rule and ADMET

The metal complex compounds were modeled in 3D, and the structure files were then converted to the "smile" format using the Open Babel GUI application. For Lipinski's Rule of 5 evaluation, the smiles files were uploaded to the SwissADME online platform (http://www.swissadme.ch/), and the "Run" button was clicked to obtain the corresponding Lipinski parameters. For ADMET analysis, the smiles files were uploaded to the pkCSM online server (https://biosig.lab.uq.edu.au/pkcsm/prediction), and the "ADMET" button was selected to retrieve data on absorption, distribution, metabolism, excretion, and toxicity [19].

Molecular Docking

The molecular docking study commenced with the retrieval of the crystal structure bearing PDB ID 2X23 from the Protein Data Bank (https://www.rcsb.org/structure/2X23). The compound 5-hexyl-2-(2-methylphenoxy)phenol was employed as a positive control [20]. Four ligands were selected for docking, namely Ni(II)Ser-Tyr Dtc, Zn(II)Ser-Tyr Dtc, Ser-Tyr Dtc and isoniazid (INH). Preparation of the protein and the reference ligand was conducted using YASARA software, which involved the removal of non-essential components such as bound ligands, cofactors, and water molecules. Ligand preparation was performed using MarvinSketch at physiological pH (7.4), and the initial structures were saved in *.mrv* format. Subsequently, the *.mrv* files were reopened in MarvinSketch, and a conformational search was carried out using the "Conformers Search" function to generate multiple low-energy conformers. The resulting structures were exported in *.mol2* format. Both protein and ligand files were then subjected to molecular docking using the PLANTS software, with *protein.mol2* and *ligand.mol2* as the respective input files. The docking pose yielding the highest score was considered to represent the most probable binding orientation of the ligand within the active site of the target protein. Based on this pose, the root-mean-square deviation (RMSD) value was calculated using YASARA. The docking

protocol was deemed valid if the RMSD value was less than 2 Å (1 Å = 10^{-10} m) [21].

Antibacterial activity

The antibacterial activities of Ni(II) Ser-Tyr Dtc and Zn(II) Ser-Tyr Dtc metal complexes were evaluated against *M. tuberculosis* H37Rv. Initially, the bacterial strain was revitalized by inoculating it into Lowenstein-Jensen (LJ) medium with 5 drops of the bacterial suspension, followed by incubation at 37 °C for 4 - 6 weeks. Antibacterial efficacy was assessed using the standard LJ protocol. Sterile LJ media were supplemented with isoniazid (positive control), dimethyl sulfoxide (DMSO; negative control), and various concentrations of the metal complexes, then incubated at 37 °C for 8 weeks.

Bacterial growth was monitored visually by examining the appearance of colonies on the LJ medium. The presence of rough, granular, creamy white to yellowish colonies indicated positive bacterial growth, whereas the absence of visible colonies on the slanted medium after 8 weeks of incubation indicated no bacterial growth. Growth was observed weekly or every 10 days and assessed qualitatively using the following scale: – (no growth), + (slight growth), ++ (moderate growth), and +++ (confluent growth). The minimum inhibitory concentration (MIC) was defined as the lowest concentration of each metal complex that completely inhibited visible bacterial growth on the LJ medium.

Results and discussion

Based on the information presented in **Table 1**, the resulting complex compounds exhibited high yields, indicating a strong and stable coordination bond between the metal and the ligand. The stability of the metal-ligand bond is further supported by the high melting point, with a difference of ≤ 2 °C [22]. The conductivity value, which is below 65 S/m, suggests that the complex compound is a non-electrolyte and remains stable [23].

Table 1 Physicochemical characteristics of the synthesized metal complexes

Compounds	Color	Yield (%)	Melting Point (°C)	Conductivity (S/m)
Ser-Tyr Dtc	yellowish white	57.32	204 - 206	0.001
Ni(II) Ser-Tyr Dtc	greenish white	57.72	237 - 239	0.038
Zn(II) Ser-Tyr Dtc	white	68.77	210 - 212	0.008

UV-Vis characterization

The UV-Vis spectroscopic analysis of the Ni(II) Ser-Tyr Dtc and Zn(II) Ser-Tyr Dtc complexes is presented in **Figure 4**. Band I exhibited a shift within the range of 276 - 423 nm for the Ni(II) complex and 274 - 437 nm for the Zn(II) complex, corresponding to an intraligand $n \rightarrow \pi^*$ transition associated with the CS_2 group. Complexes containing C=S moieties typically display intense absorption bands in the 250 - 320 nm region, attributed to $\pi \rightarrow \pi^*$ and $n \rightarrow \pi^*$ electronic transitions [24,25]. In dithiocarbamate-based complexes, absorption in the 310 - 400 nm range is indicative of $n \rightarrow \pi^*$ transitions within the N=C=S group. Additional absorption bands observed at 400 - 423 nm for Ni(II) and 400 - 437 nm for Zn(II) complexes suggest the occurrence of charge transfer (CT) transitions between the ligand and metal center (ligand-to-metal and metal-to-ligand). Furthermore, absorption in the 643 - 674 nm range for Ni(II) and 530 - 697 nm for Zn(II) indicates an extended conjugation system in the complexes compared to the free ligands, as well as the presence of d-d transitions characteristic of transition metal complexes [26]. These observations collectively confirm the formation of metal-ligand bonds in the synthesized complexes.

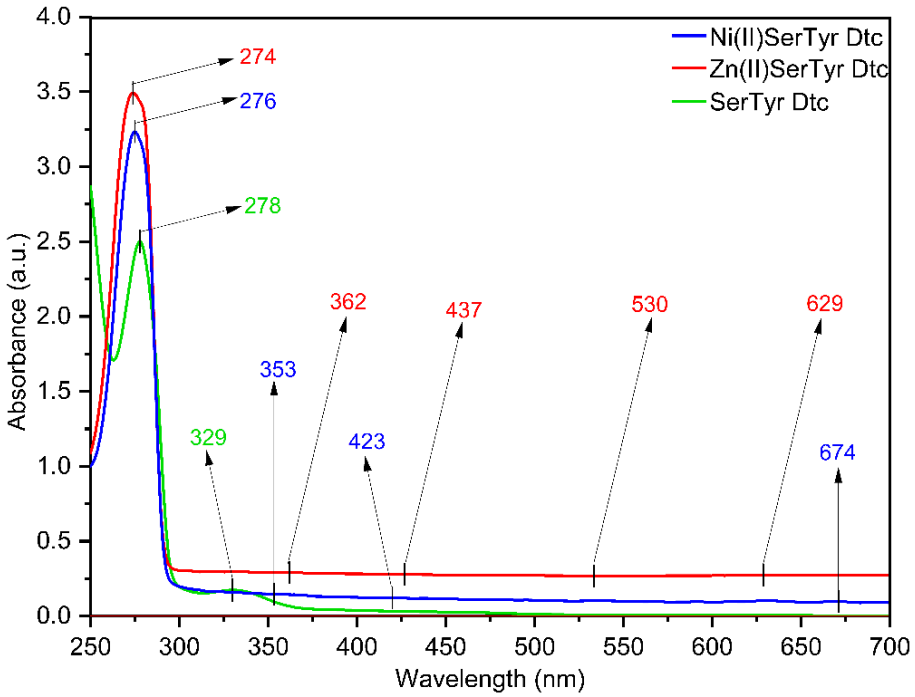

Figure 4 UV-Vis absorption spectrum of Ser-Tyr Dtc, Ni(II) and Zn(II) serine-tyrosine dithiocarbamate complexes.

FTIR Characterization

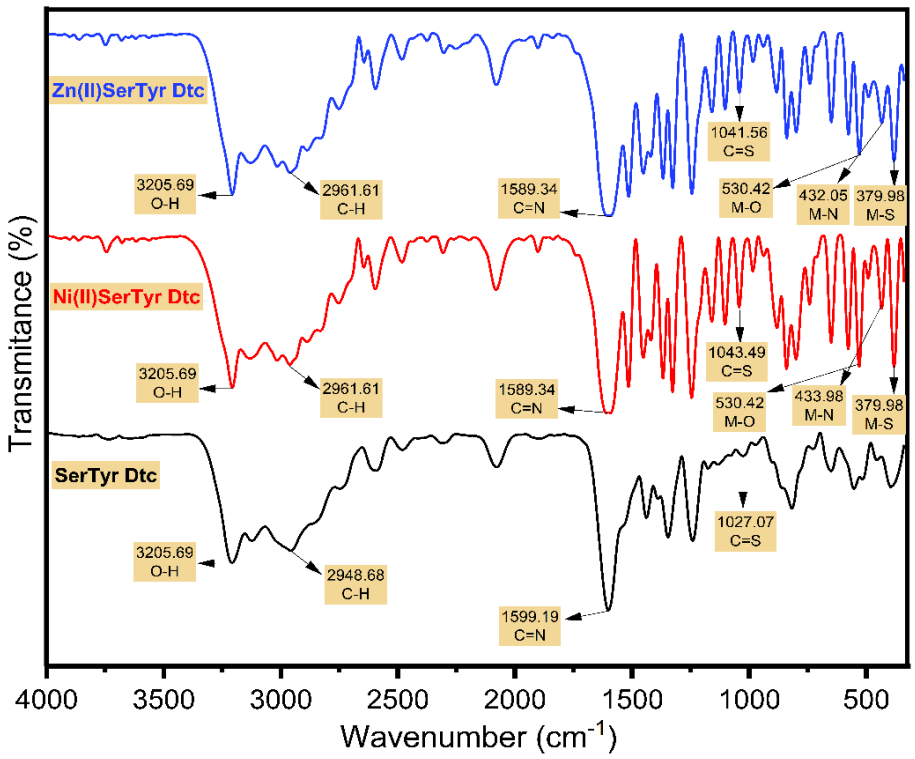

Figure 5 FTIR spectrum of Ser-Tyr Dtc, Ni(II) and Zn(II) serine-tyrosine dithiocarbamate complexes.

Fourier Transform Infrared (FT-IR) spectroscopy was conducted in the wavenumber range of 4,000 - 300 cm^{-1} to identify the characteristic absorption bands of Ni(II) Ser-Tyr Dtc and Zn(II) Ser-Tyr Dtc (**Figure 5**).

An absorption band observed at 3205.69 cm^{-1} corresponds to the stretching vibration of hydroxyl groups (Ar–OH) from the aromatic moiety, indicating their involvement in complex formation [27-29]. The peak at 1514.12 cm^{-1} is attributed to the C=N stretching vibration. Absorption bands at 1043.49 cm^{-1} for Ni(II) Ser-Tyr Dtc and 1041.56 cm^{-1} for Zn(II) Ser-Tyr Dtc confirm the presence of C=S groups from the dithiocarbamate ligands and suggest bidentate coordination of the C=S group to the metal center. The band at 379.98 cm^{-1} corresponds to metal–sulfur (M–S) interactions. Additionally, new absorption peaks at 433.98 cm^{-1} for Ni(II) and 432.05 cm^{-1} for Zn(II) are indicative of metal–nitrogen (M–N) bonding [30,31]. The absorption at 530.42 cm^{-1} further supports the presence of metal–oxygen (M–O) interactions. The FT-IR spectra clearly show the coordination of Ni(II) and Zn(II) ions with Ser-Tyr Dtc ligands. The observed M-S (≈380 cm^{-1}), M-N (≈433 cm^{-1}), and M-O (≈530 cm^{-1}) bands confirm the direct metal binding to the sulfur atom of the dithiocarbamate group, nitrogen of the peptide backbone, and oxygen of the tyrosine hydroxyl group. The shifts and new peaks appearing on the Ni(II) and Zn(II) complexes compared to the free ligands indicate successful complexation. A summary of the FT-IR spectral data for the synthesized complexes is presented in **Table 2**.

Table 2 Infrared absorption data of metal complex compounds.

Compound/Funcional group	Ser-Tyr Dtc	Ni(II) Ser-Tyr Dtc	Zn(II) Ser-Tyr Dtc
v(M-S) cm^{-1}	-	379.98 s	379.98 m
v(M-N) cm^{-1}	-	433.98 w	432.05 w
v(M-O) cm^{-1}	-	530.42 s	530.42 m
v(C=S) cm^{-1}	1027.07 m	1043.49 m	1041.56 m
v(C=N) cm^{-1}	1599.19 s	1589.34 s	1589.34 s
V(C-H) cm^{-1}	2948.68 m	2961.61 m	2961.61 m
v(O-H) cm^{-1}	3205.69 s	3205.69 s	3205.69 s

s = strong; m = medium; w = weak

XRD characterization

The diffractograms obtained from X-ray Diffraction (XRD) analysis illustrate the crystalline nature of the synthesized complexes, as evidenced by the appearance of sharp diffraction peaks at 2θ regions around (17, 83°, 20.10°, 24.56°, 44.05°, and 64.43°) for Ni(II)Ser-Tyr Dtc and (17.82°, 20.09°, 24.55°, 44.05°, and 64.42°) for Zn(II)Ser-Tyr Dtc indicating an orthorhombic crystal system. The formation of this well-defined crystal structure is due to the coordination interaction between the metal ion and ligand during complexation. The crystallinity of the compound is further supported by the physical characteristics of the synthesized product, which appears as a yellowish-white solid (**Figure 6**).

.

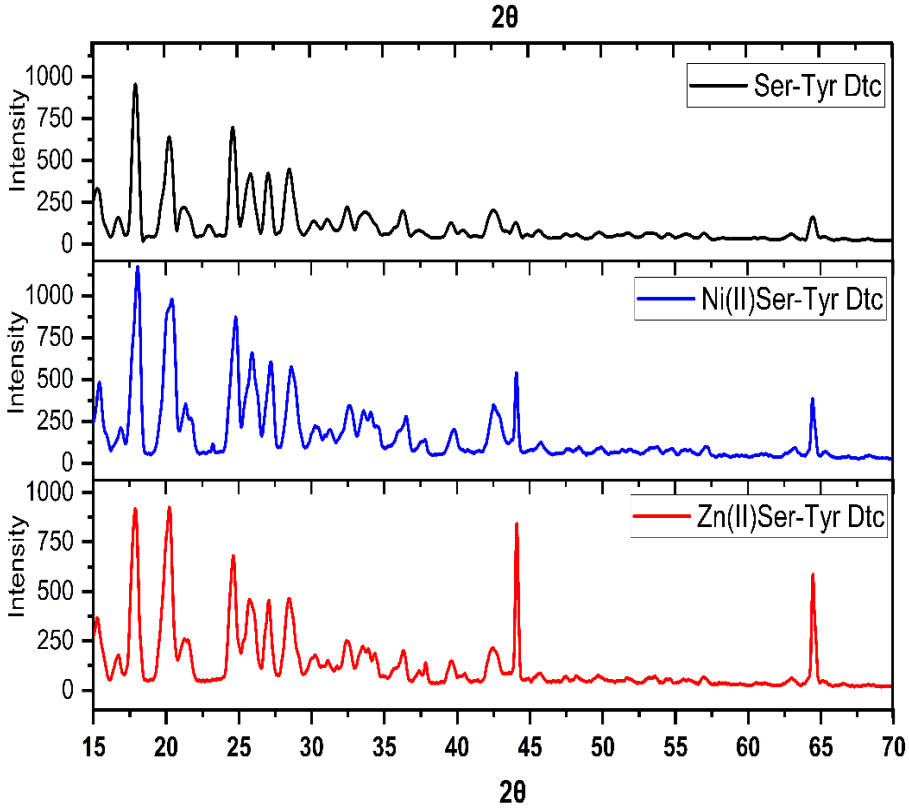

Figure 6 XRD diffractogram of Ser-Tyr Dtc, Ni(II) and Zn(II) serine-tyrosine ditiocarbamate complexes.

SEM-EDS characterization

Surface morphology analysis using Scanning Electron Microscopy (SEM) at 1,000× magnification revealed that both Ni(II) Ser-Tyr Dtc and Zn(II) Ser-Tyr Dtc complexes exhibit orthorhombic crystal structures, along with the presence of surface impurities and irregular particle distributions (**Figure 7**). Elemental composition was further confirmed through Energy Dispersive X-ray Spectroscopy (SEM-EDS) analysis (**Figure 8**), which detected the presence of carbon (C), oxygen (O), nitrogen (N), sulfur (S), and the respective metal ions (Ni and Zn) in the samples. The EDS spectrum of the Ni(II) Ser-Tyr Dtc complex indicated the following elemental composition: Ni (24.96%), C (8.88%), O (12.11%), N (2.27%), and S (51.33%). Meanwhile, the Zn(II) Ser-Tyr Dtc complex showed Zn (16.12%), C (47.56%), O (26.31%), N (3.83%), and S (6.17%). These results confirm the successful incorporation of Ni(II) and Zn(II) ions into the Ser-Tyr DTC ligand, indicating the formation of metal-ligand complexes.

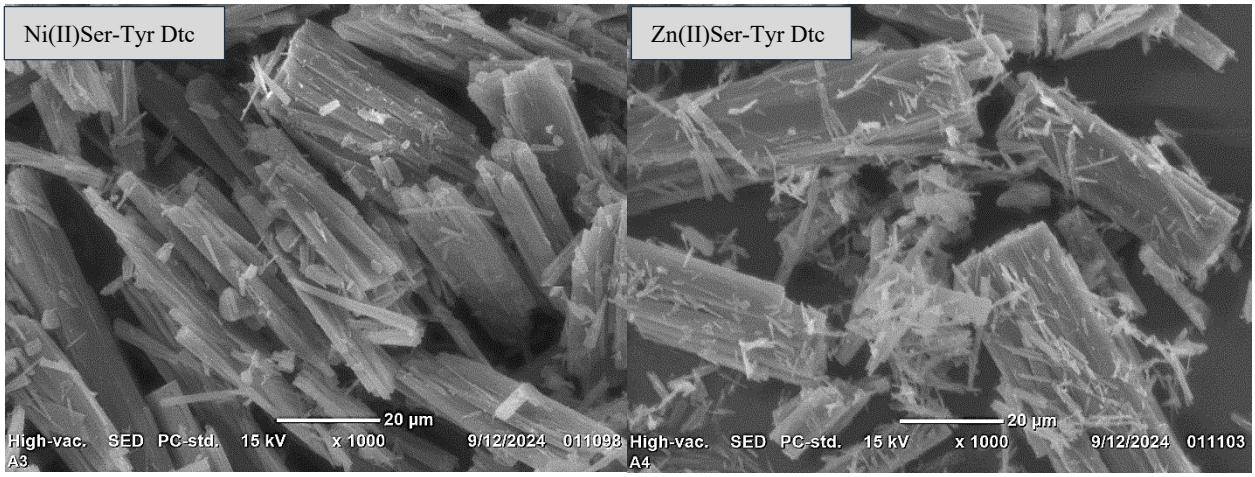

Figure 7 SEM Morphology of Ni(II) and Zn(II) serine-tyrosine ditiocarbamate complexes.

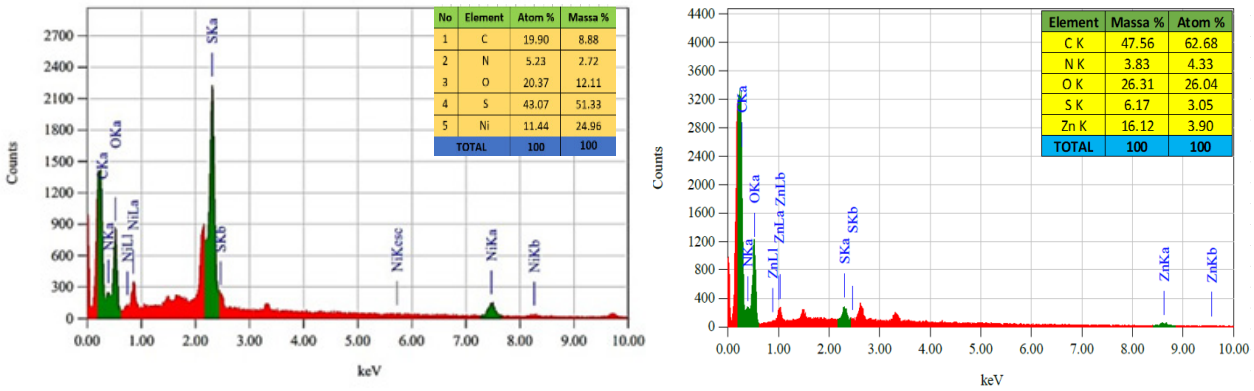

Figure 8 SEM-EDS of Ni(II) and Zn(II) serine-tyrosine ditiocarbamate complexes.

Lipinski rule and ADMET analysis results

Lipinski's Rule of 5 is widely employed to identify potential drug-like compounds [32]. This rule assists in predicting the biological and pharmacokinetic suitability of a compound based on its physicochemical properties, which influence its potential to act as an orally active drug in humans. According to this guideline, a compound is considered a viable oral drug candidate if it satisfies at least 3 out of the 5 specified criteria [33]. The evaluation results of the tested compounds based on Lipinski's parameters are presented in **Table 3**.

Table 3 Lipinski's rule analysis results of synthesized compounds.

Compounds	Molecular Weight (g/mol)	Log P	Donor H	Akseptor H
Ni(II)Ser-Tyr Dtc	400.08	0.17	2	6
Zn(II)Ser-Tyr Dtc	407.77	0.05	3	6
Ser-Tyr Dtc	344.41	0.57	5	5
Isoniazid (INH)	137.14	−0.35	2	3
Value requirement	**≤ 500**	**≤ 5**	**≤ 5**	**≤ 10**

Based on **Table 3**, chemical compounds capable of penetrating biological cell membranes typically possess a molecular weight below 500 g/mol. Exceeding this threshold generally reduces the compound's ability to diffuse across the membrane [34]. The log *p*-value represents the lipophilicity of a compound, indicating its solubility in a biphasic system such as octanol and water. Negative log *p*-values reflect a relatively

hydrophilic nature, which enhances solubility in aqueous environments but may hinder membrane permeability. In contrast, moderately positive log *p*-values suggest a favorable balance between aqueous solubility and membrane permeability. However, excessively high log *p*-values indicate strong lipophilicity, which increases the compound's tendency to dissolve in hydrophobic environments, such as lipid bilayers [35]. This can lead to a higher toxicity profile due to prolonged retention in lipid membranes, resulting in tissue accumulation and reduced selectivity toward specific biological targets, such as enzymes or receptors. Furthermore, the number of hydrogen bond donors and acceptors is associated with the compound's ability to form hydrogen bonds. An increased number of these groups often correlates with higher energy requirements during the absorption process [36]. As shown in **Table 3**, all designed compounds satisfy the criteria of Lipinski's Rule, indicating favorable potential as oral drug candidates. Therefore, subsequent analysis proceeded to the evaluation of their ADMET (Absorption, Distribution, Metabolism, Excretion, and Toxicity) profiles. The results of the ADMET analysis for the complex compounds are presented in **Table 4**.

Table 4 ADMET analysis results using pkCSM.

Property	Model name	INH	Ser-Tyr Dtc	Ni(II)Ser-Tyr Dtc	Zn(II)Ser-Tyr Dtc	Unit
Absorption	Water solubility	0.09	−2.703	−3.514	−2.866	mol/L
	Caco2 permeability	0.153	−0.359	0.243	0.235	Papp in 10^{-6} cm/s
	Intestinal absorption (human)	82.954	21.66	89.485	76.553	% Absorbed
	Skin Permeability	−3.496	−2.735	−3.598	−3.255	Kp
	P-glycoprotein substrate	Yes	Yes	Yes	Yes	Yes/No
	P-glycoprotein I inhibitor	No	No	No	No	Yes/No
	P-glycoprotein II inhibitor	No	No	No	No	Yes/No
Distribution	VDss (human)	−0.348	−1.596	−0.163	0.027	L/kg
	Fraction unbound (human)	0.635	0.578	0.402	0.475	Fu
	BBB permeability	0.004	−1.633	−1.048	−1.176	BB
	CNS permeability	−2.784	−3.704	−3.032	−3.644	PS
Metabolism	CYP2D6 substrate	No	Yes	No	No	Yes/No
	CYP3A4 substrate	No	No	Yes	No	Yes/No
	CYP1A2 inhibitior	No	No	No	No	Yes/No
	CYP2C19 inhibitior	No	No	No	No	Yes/No
	CYP2C9 inhibitior	No	No	No	No	Yes/No
	CYP2D6 inhibitior	No	No	No	No	Yes/No
	CYP3A4 inhibitior	No	No	No	No	Yes/No
Excretion	*Total Clearance*	0.718	0.105	−0.289	−0.453	mL/min/kg
	Renal OCT2 substrate	No	No	No	No	Yes/No

Property	Model name	INH	Ser-Tyr Dtc	Ni(II)Ser-Tyr Dtc	Zn(II)Ser-Tyr Dtc	Unit
Toxicity	AMES toxicity	No	No	Yes	No	Yes/No
	Max. tolerated dose (human)	1.407	1.006	−0.223	−1.273	mg/kg/day
	hERG I inhibitor	No	No	No	No	Yes/No
	hERG II inhibitor	No	No	No	No	Yes/No
	Oral Rat Acute Toxicity (LD_{50})	2.436	2.05	2.931	2.427	Mol/kg
	Oral Rat Chronic Toxicity (LOAEL)	2.433	2.225	1.356	1.413	mg/kg_ bw/day
	Hepatotoxicity	No	Yes	No	No	Yes/No
	Skin Sensitisation	No	No	No	No	Yes/No
	T.Pyriformis toxicity	−0.512	0.285	0.325	0.342	ug/L
	Minnow toxicity	3.387	2.372	1.895	2.049	mM

Based on **Table 4**, the water solubility of all compounds ranges from –3.514 to 0.09, indicating low solubility in water and a tendency to dissolve in non-polar solvents [19]. However, these values are still above the minimum limit for oral drug candidates (> −6) [37]. Caco-2 permeability values for all compounds were below the required threshold of 0.9, including INH (0.153), suggesting low intestinal permeability [19]. Despite this, all compounds except the ligand showed good human intestinal absorption, exceeding the standard of 30% [38]. Skin permeability values ranged from –3.598 to –2.735, which indicates low transdermal absorption and supports oral use [39]. All compounds were predicted to be P-gp substrates but not inhibitors, indicating low risk of transporter-related toxicity or drug interactions [40].

The distribution analysis shows that the complexes and INH have low VDss values (–1.596 to 0.027). According to pkCSM, log VDss values < −0.15 are considered low, while > 0.45 are considered high [19]. Based on this, only the Zn(II) complex falls within the acceptable range, while ligand, Ni(II) and INH do not. The fraction of unbound drug (Fu) shows how much of the compound is free in plasma. All compounds had Fu values between 0.402 to 0.635, indicating they are pharmacologically active (Fu > 0.1) [41]. In terms of blood–brain barrier (BBB) penetration, only INH showed a borderline log BB value (0.004), while the others were below –1, suggesting they do not cross the BBB-an advantage for drugs not targeting the brain [39]. CNS permeability (log PS < –2) was observed in all compounds, indicating low brain penetration and reduced risk of neurotoxicity.

All compounds did not inhibit major CYP enzymes (CYP1A2, CYP2C19, CYP2C9, CYP2D6, and CYP3A4) except the ligand, which is beneficial as it lowers the risk of drug interactions [42]. The Ni(II) complex was found to be a substrate of CYP3A4, which is still acceptable if it does not cause excessive enzyme competition. In general, the absence of CYP inhibition indicates good metabolic safety, reducing the risk of toxicity and interactions with other drugs [43]. Thus, all compounds showed favorable metabolic profiles as potential drug candidates.

Excretion is the process of eliminating waste or toxic substances from the body, mainly through the kidneys or liver [44]. Total clearance reflects how efficiently a compound is removed from the body, combining renal and hepatic clearance. A low clearance value indicates higher risk of compound accumulation. Renal excretion involves the Organic Cation Transporter 2 (OCT2), which facilitates drug removal via urine. Based on **Table 4**, all compounds showed low total clearance and were not OCT2 substrates, suggesting limited renal excretion and a higher potential for accumulation [39].

The AMES test evaluates a compound's potential mutagenicity using bacteria [19,39]. The Ni(II) complex tested positive, indicating possible mutagenic activity, while ligand, Zn(II) and INH were negative. Based on **Table 4**, all metal complexes had negative bioactivity values, suggesting low biological activity, while INH showed a value of 1.407 and ligand 1.006, indicating it is likely active at the intended dose. All compounds tested negative as hERG I and II inhibitors, suggesting low risk of causing ventricular arrhythmias [45]. All compounds, except for ligands, showed no signs of hepatotoxicity or skin sensitization, indicating good liver and skin safety [19]. Regarding environmental toxicity, all compounds were within the safe range for *T. pyriformis* (log µg/L > −0.5), but exceeded the toxicity threshold for Minnow (log mM < −0.3), indicating potential toxicity to that species.

Molecular docking of metal complex on enoyl-ACP reductase

In this study, redocking produced the best conformation in conformation 1, with the lowest RMSD value of 1.6791 Å. Enoyl-ACP reductase was selected as the primary target for tuberculosis therapy due to its essential role in the biosynthesis of mycolic acid, a major component of the *Mycobacterium tuberculosis* cell wall (strain ATCC 25618/ H37Rv) [46]. The interaction between the synthesized complexes and this enzyme is expected to disrupt mycolic acid synthesis, leading to cell wall damage and inhibition of bacterial growth. Docking scores and interaction patterns for the positive control 5-Hexyl-2-(2-Methylphenoxy)Phenol, Ni(II)Ser-Tyr Dtc, Zn(II)Ser-Tyr Dtc, and INH with Enoyl-ACP reductase are shown in **Table 5** and **Figures 9 - 13**.

Table 5 Docking score of metal complexes.

Compounds	Score docking
Control 5-Hexyl-2-(2-Methylphenoxy)Phenol	−98.8828 kJ/mol
Ni(II)Ser-Tyr Dtc	−95.0923 kJ/mol
Zn(II)Ser-Tyr Dtc	−89.1673 kJ/mol
Ser-Tyr Dtc	−98.49 kJ/mol
INH	−65.8232 kJ/mol

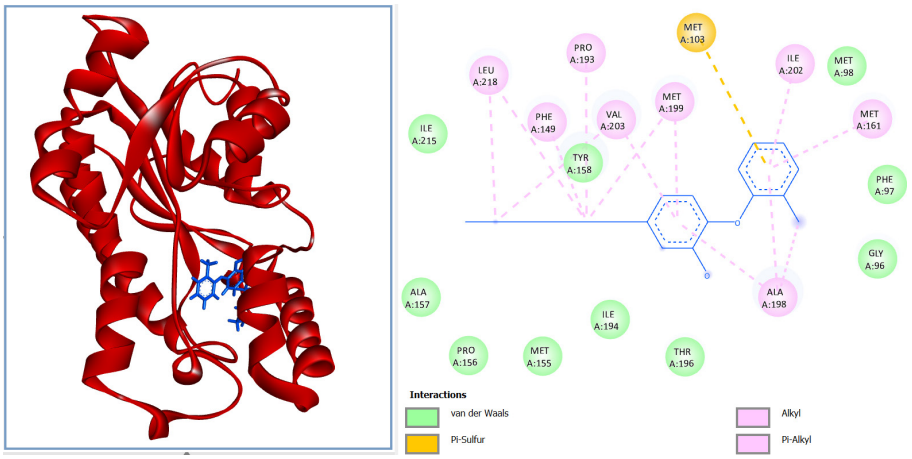

Figure 9 Docking visualization of 5-Hexyl-2-(2-Methylphenoxy)Phenol (control+) on Enoyl-ACP reductase.

The positive control compound, 5-Hexyl-2-(2-Methylphenoxy)Phenol, showed strong binding to Enoyl-ACP reductase with a binding energy of −98.8828 kJ/mol, indicating high affinity and stable complex formation. It formed multiple hydrophobic interactions (alkyl and π-alkyl) with key active site residues such as LEU A:218, PHE A:149, PRO A:193, VAL A:203, MET A:199, ALA A:198, MET A:161, and

ILE A:202. Additionally, π-sulfur interactions were observed with MET A:103, along with several van der Waals interactions, further stabilizing the ligand-enzyme complex.

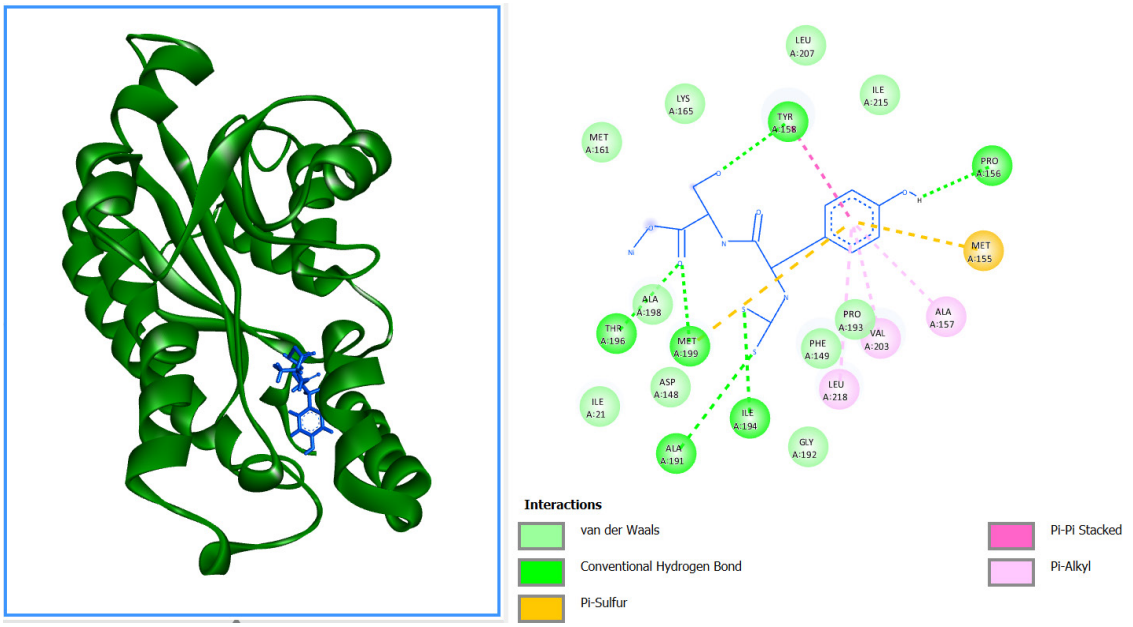

Figure 10 Docking visualization of Ni(II)Ser-Tyr Dtc on Enoyl-ACP reductase.

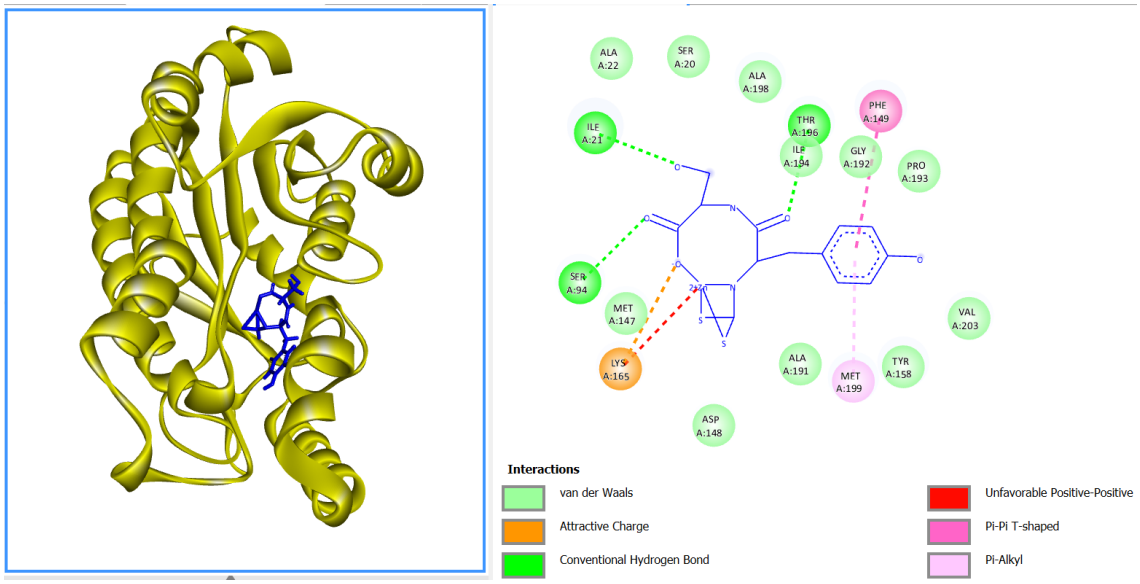

Figure 11 Docking visualization of Zn(II)Ser-Tyr Dtc on Enoyl-ACP reductase.

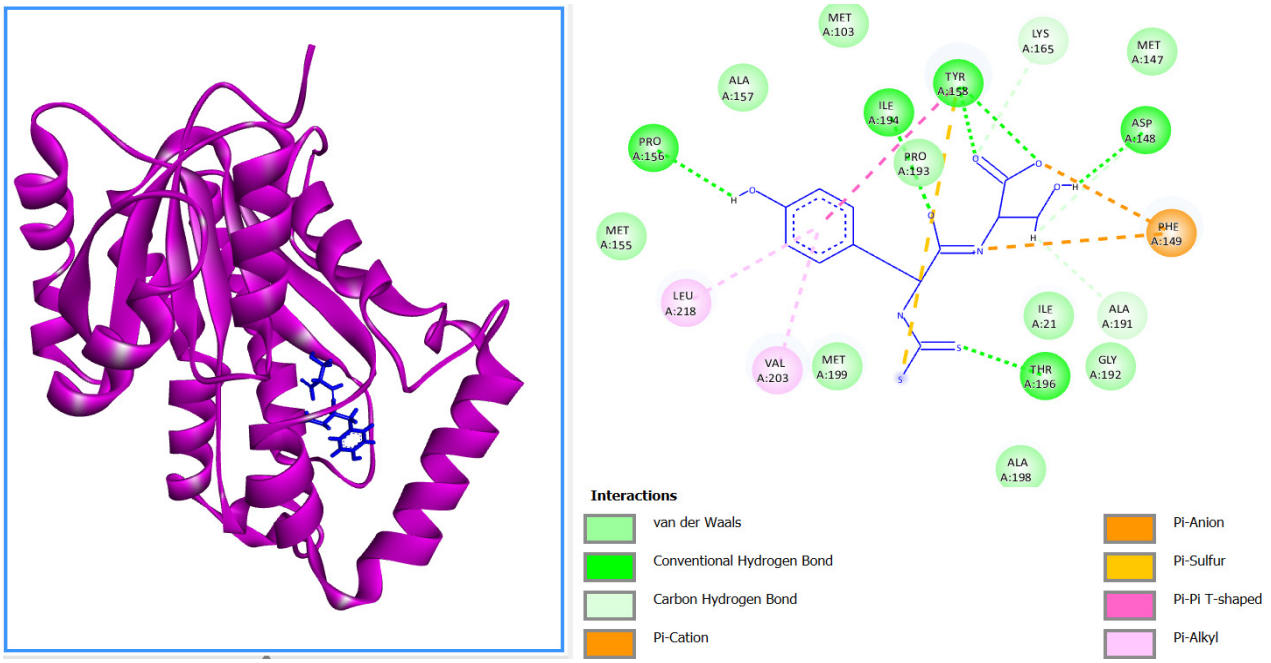

Figure 12 Docking visualization of Ser-Tyr Dtc on Enoyl-ACP reductase.

The Ni(II)Ser-Tyr Dtc complex showed a binding energy of −95.0923 kJ/mol with Enoyl-ACP reductase, indicating strong affinity and stable complex formation. It formed conventional hydrogen bonds with residues THR A:196, MET A:199, ALA A:191, ILE A:194, TYR A:158, and PRO A:156, enhancing ligand stability at the active site. Additional interactions included π-sulfur with MET A:155, along with π-π stacking and π-alkyl interactions contributing to hydrophobic binding (**Figure 10**). The Zn(II)Ser-Tyr Dtc complex showed a binding energy of −89.1673 kJ/mol, indicating fairly strong affinity for Enoyl-ACP reductase. The complex is stabilized by hydrogen bonds with ILE A:21, SER A:94, and THR A:196. It also forms π-π T-shaped interaction with PHE A:149, π-alkyl interaction with MET A:199, and electrostatic interaction with LYS A:165, contributing to binding stability. Additional van der Waals interactions with nearby residues further support the complex structure. One unfavorable positive-positive interaction was also observed (**Figure 11**).

The Ser-Tyr Dtc compound showed the lowest binding energy of -98.49 kJ/mol, indicating high affinity to the Enoyl-ACP reductase protein. Conventional hydrogen interactions with residues PRO A:156, THR A:196, ILE A:194, TYR A:158, and ASP A:148 also strengthen the stability of the ligand-protein complex. In addition, there are π-anion, π-cation (with PHE A:149), π-π T-shaped, and π-alkyl interactions that indicate the involvement of aromatic binding, as well as other additional interactions (**Figure 12**). Despite showing the highest binding affinity, the Ser-Tyr Dtc compound is potentially toxic, especially to the liver based on the results of ADMET analysis. This confirms that high affinity does not always go hand in hand with biological safety, hence the need for structural modifications to reduce the risk of toxicity. Molecular docking results show that all designed metal complexes interact with Enoyl-ACP reductase, each involving different active site residues. This indicates their potential as Enoyl-ACP reductase inhibitors. Additionally, the complexes demonstrated better binding affinity than Isoniazid (INH), a known anti-TB drug, which had a lower docking score of −65.8232 kJ/mol. The docking results for INH are shown in **Figure 13**. The main interactions on INH compounds involve conventional hydrogen bonds with ILE residue A:194 and π-π T-shaped interactions with PHE A:149.

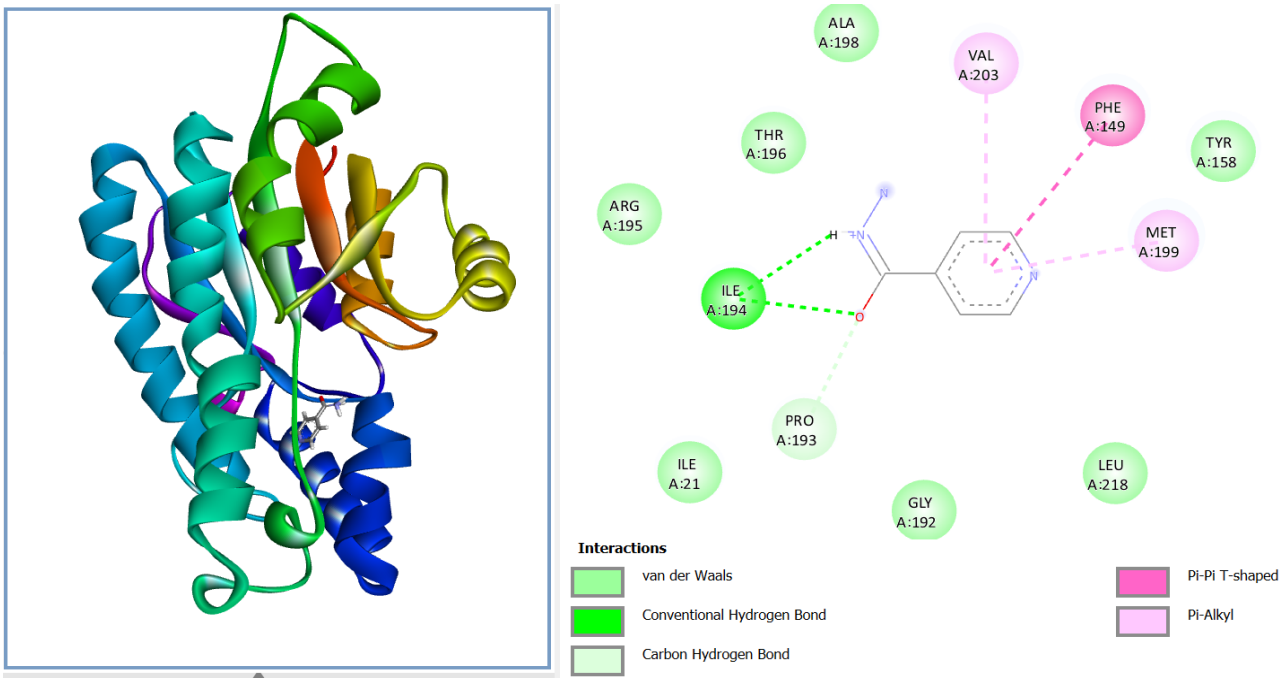

Figure 13 Docking visualization of INH on Enoyl-ACP reductase.

Antituberculosis activity of metal complex compounds

The inhibitory activity of the synthesized metal complexes against *M. tuberculosis* H37Rv was assessed over an 8-week period. Isoniazid serves as a positive control because its mechanism is similar to metal complexes in that it targets the bacterial cell wall by interacting with oxygen atoms on the hydroxyl and carbonyl groups of mycolic acid [47]. Week 8 inhibition results are shown in **Figure 14** and **Table 6**. DMSO was used as a negative control since it lacks antibacterial properties, allowing normal bacterial growth [48]. The antituberculosis effect depends on disrupting the structure of mycolic acid in the bacterial cell wall. Metal ions can bind to hydroxyl and carbonyl oxygen atoms in mycolic acid. In this study, dithiocarbamate ligands acted as chelators, enabling metal interaction with mycolic acid and weakening the bacterial cell wall [49].

Figure 14 Antituberculosis test results (X) DMSO negative control, (Y) INH positive control, (L) Ser-Tyr Dtc ligand L1-L5, (A) Ni(II)Ser-Tyr Dtc B1-B5, and (B) Zn(II)Ser-Tyr Dtc C1-C5.

Table 6 Results of LJ test observations.

Compounds	Consentration (mg/L)	Observation of colony growth of *M. tuberculosis* H37Rv					
		d^{10}	d^{20}	d^{30}	d^{40}	d^{50}	d^{60}
DMSO (negative control)	4000	–	–	+	++	+++	+++
Isoniazid (positive control)	4000	–	–	–	–	–	–
Ser-Tyr Dtc L1	150	–	–	–	***	***	***
Ser-Tyr Dtc L2	250	–	–	–	–	–	–
Ser-Tyr Dtc L3	500	–	–	–	***	***	***
Ser-Tyr Dtc L4	1000	–	–	–	–	–	–
Ser-Tyr Dtc L5	1500	–	–	–	–	–	–
Ni(II)Ser-Tyr Dtc B1	150	–	–	–	–	–	–
Ni(II)Ser-Tyr Dtc B2	250	–	–	–	–	–	–
Ni(II)Ser-Tyr Dtc B3	500	–	–	–	–	–	–
Ni(II)Ser-Tyr Dtc B4	1000	–	–	–	–	–	–
Ni(II)Ser-Tyr Dtc B5	1500	–	–	–	–	–	–

Compounds	Consentration (mg/L)	Observation of colony growth of *M. tuberculosis* H37Rv					
		d^{10}	d^{20}	d^{30}	d^{40}	d^{50}	d^{60}
Zn(II)Ser-Tyr Dtc C1	150	–	–	–	–	–	–
Zn(II)Ser-Tyr Dtc C2	250	–	–	–	–	–	–
Zn(II)Ser-Tyr Dtc C3	500	–	–	–	–	–	–
Zn(II)Ser-Tyr Dtc C4	1000	–	–	–	–	–	–
Zn(II)Ser-Tyr Dtc C5	1500	–	–	–	–	–	–

Description : + = slight growth; *** = contaminated (spoiled)
++ = moderate growth; – = sensitive (no growth)
+++ = confluent growth (resistant); d^x = day-x

The synthesized metal complexes showed strong antituberculosis activity, indicated by the absence of *M. tuberculosis* colonies (no yellow color or granular spots on the media). However, contamination was observed in 2 Ser-Tyr Dtc ligands (L1 at 150 mg/L and L3 at 500 mg/L), likely due to microbial overgrowth turning the media fully yellow. Notably, 2 ligand-only samples (Ser-Tyr Dtc L1 and L3 at 150 and 500 mg/L) exhibited a uniformly yellow medium, suggesting possible microbial contamination. These findings may reflect instability of the free ligand under test conditions or technical error during sample preparation. These contaminated samples were excluded from the interpretation of the antimicrobial results. Importantly, none of the metal complex samples showed signs of contamination. The absence of *M. tuberculosis* growth at the lowest tested concentration (150 ppm) suggests that the MIC value of the metal complexes is lower than 150 ppm. However, further studies using lower concentration ranges (e.g., 10–150 ppm) are needed to determine the exact MIC value.

Conclusions

The Ni(II)Ser-Tyr Dtc and Zn(II)Ser-Tyr Dtc complexes were successfully synthesized via an *in situ* method, yielding solid products. The synthesis yields were 57.22% for Ni(II)Ser-Tyr Dtc and 68.77% for Zn(II)Ser-Tyr Dtc. The metal complexes were characterized using FT-IR, UV-Vis, XRD, and SEM-EDS, all confirming their structural features. The formation of the metal complexes was confirmed by SEM-EDS through elemental identification, while FT-IR, UV-Vis, and XRD analyses provided supportive evidence for their structural characteristics. Molecular docking revealed strong interactions with the target enzyme Enoyl-ACP reductase, primarily through hydrogen bonding. The Ni(II)Ser-Tyr Dtc complex achieved the highest docking score (-95.0923 kJ/mol), outperforming the standard drug isoniazid (INH), which scored −65.8232 kJ/mol. *In vitro* tests using the Lowenstein–Jensen method also showed effective inhibition, with no *M. tuberculosis* H37Rv colony growth observed.

Acknowledgements

The authors would like to thank the Inorganic and Organic Research Center Laboratory, the Integrated Chemistry Laboratory, the Science Research and Development Laboratory, and the Microbiology Laboratory of the Faculty of Medicine, Hasanuddin University, Makassar, Indonesia, for their support of this research.

Declaration of Generative AI in Scientific Writing

- This manuscript utilized generative AI tools, namely ChatGPT (OpenAI) and Grammarly, to enhance language clarity, grammar, and overall readability.
- All AI-assisted edits were made under strict human oversight and control.
- These tools were not used to Generate scientific content, Interpret or analyze data, Develop research questions, Draw or formulate conclusions.
- The authors are responsible for the manuscript's intellectual content, scientific accuracy, and integrity.

CRediT Author Statement

Wildan Mubaraq: Conceptualization, Methodology, Writing –Original Draft, Visualization. **Indah Raya:** Supervision, Project Administration, Writing –Review & Editing, Funding Acquisition. **Herlina Rasyid:** Investigation, Resources, Writing – Review & Editing. **Nunuk Hariani Soekamto:** Validation, Formal Analysis, Writing – Review & Editing. **Hasnah Natsir:** Methodology, Software, Data Curation. **Djabal Nur Basir:** Investigation, Resources. **Rizal Irfandi:** Software, Formal Analysis, Visualization. **Bulkis Musa:** Data Curation, Investigation. **Erna Mayasari:** Writing –Review & Editing, Validation. **Wanda Wardyanti:** Data Curation, Software. **Andi Adillah Nur Syafirah:** Software, Visualization, *In Vitro* analysis. **Desy Kartina:** Formal Analysis, Visualization. **Santi Santi:** Writing –Review, Visualization.

References

[1] World Health Organization. *Global Tuberculosis Report 2023*. Geneva, Switzerland, 2024.

[2] AJ Reis, JLD Pizzol, R Gattelli, AV Groll, DF Ramos, IB Ramis, A Kritski, JRLE Silva and PEAD Silva. Thesis and dissertations examining tuberculosis in brazil between 2013 and 2019: An overview. *Journal of the Brazilian Society of Tropical Medicine* 2022; **55**, e0198-e2022.

[3] I Gajic, N Tomic, B Lukovic, M Jovicevic, D Kekic, M Petrovic, M Jankovic, A Trudic, DM Culafic, M Milenkovic and N Lukovic. A comprehensive overview of antibacterial agents for combating multidrug-resistant bacteria: the current landscape, development, future opportunities, and challenges. *Antibiotics* 2025; **14(3)**, 221.

[4] MN Patel, AJ Patel, MN Nandpal, MA Raval, RJ Patel, AA Patel, KR Paudel, PM Hansbro, SK Singh, G Gupta, K Dua and SG Patel. Advancing against drug-resistant tuberculosis: an extensive review, novel strategies and patent landscape. *Naunyn-Schmiedeberg's Archives of Pharmacology* 2025; **398**, 2127-2150.

[5] K Srinivasulu, KH Reddy, K Anuja, D Dhanalakshmi and YB Nagamani. Design, synthesis, spectral characterization, dna binding and antibacterial studies of ternary metal complexes with 1,10 phenanthroline and 2-acetylthiophene-4-phenyl-3-thiosemicarbazone. *Trends in Sciences* 2022; **19(16)**, 5653.

[6] N Kumar, R Kaushal and P Awasthi. *Transition metal complexes as antibacterial agents: An overview*. Springer Nature, New York, 2025.

[7] CD Natale, ID Benedictis, AD Benedictis and D Marasco. Metal-peptide complexes as promising antibiotics to fight emerging drug resistance: New perspectives in tuberculosis. *Antibiotics* 2020; **9(6)**, 337.

[8] SK Nandanwar and HJ Kim. Anticancer and antibacterial activity of transition metal complexes. *ChemistrySelect* 2019; **4(5)**, 1706-1721.

[9] NO Boadi, M Degbevi, SA Saah, M Badu, LS Borquaye and NK Kortei. Antimicrobial properties of metal piperidine dithiocarbamate complexes against *Staphylococcus aureus* and *Candida albicans*. *Scientific African* 2021; **12**, e00846.

[10] AS Alfahdawi, MS Sawsan SE Saleh and MM Saleh. Synthesis and study of N, N' -(ethane-1,2-diyl)bis(1-phenyl methanimine) and their complex derivative with *in-vivo* and *in-vitro* Bacterial biological study. *Egyptian Journal of Chemistry* 2021; **64(6)**, 2879-2888.

[11] TA Saiyed, JO Adeyemi and DC Onwudiwe. The structural chemistry of Zinc(II) and Nickel(II) dithiocarbamate complexes. *Open Chemistry* 2021; **19(1)**, 974-986.

[12] S Balakrishnan, S Duraisamy, M Kasi, S Kandasamy, R Sarkar and A Kumarasamy. Syntheses, physicochemical characterization, antibacterial studies on potassium morpholine dithiocarbamate Nickel (II), Copper (II) metal complexes and their ligands. *Heliyon* 2019; **5(5)**, e01687.

[13] N Baartzes, T Stringer, R Seldon, DF Warner, CD Kock, PJ Smith and GS Smith. Synthesis, characterization and antimicrobial evaluation of mono- and polynuclear ferrocenyl derived amino and imino complexes. *Journal of Organometallic Chemistry* 2016; **809**, 79-85.

[14] SA Khan, W Ahmad, KS Munawar and S Kanwal. Synthesis, spectroscopic characterization and biological evaluation of Ni(II), Cu(II) and Zn(II)

complexes of diphenyldithiocarbamate. *Indian Journal of Pharmaceutical Sciences* 2018; **80(3)**, 480-488.

[15] NJ Porter, NH Christianson, C Decroos and DW Christianson. Structural and functional influence of the glycine-rich loop g302gggy on the catalytic tyrosine of histone deacetylase 8. *Biochemistry* 2016; **55(48)**, 6718-6729.

[16] S Medici, M Peana, VM Nurchi and MA Zoroddu. The involvement of amino acid side chains in shielding the nickel coordination site: An NMR study. *Molecules* 2013; **18(10)**, 12396-12414.

[17] E Kasotakis and A Mitraki. Silica biotemplating by self-assembling peptides via serine residues activated by the peptide amino terminal group. *Peptide Science* 2012; **98(6)**, 501-509.

[18] A Chollet, L Maveyraud, C Lherbet and V Bernardes-Genisson. An overview on crystal structures of inha protein: Apo-form, in complex with its natural ligands and inhibitors. *European Journal of Medicinal Chemistry* 2018; **146**, 318-343.

[19] DEV Pires, TL Blundell and DB Ascher. pkCSM: Predicting small-molecule pharmacokinetic and toxicity properties using graph-based signatures. *Journal of Medicinal Chemistry* 2015; **58(9)**, 4066-4072.

[20] MBD Avila, G Bitencourt-Ferreira and WFD Azevedo. structural basis for inhibition of enoyl-[acyl carrier protein] reductase (InhA) from *Mycobacterium tuberculosis*. *Current medicinal chemistry* 2020; **27(5)**, 745-759.

[21] EP Istyastono. Docking studies of curcumin as a potential lead compound to develop novel dipeptydyl peptidase-4 inhibitors. *Indonesian Journal of Chemistry* 2009; **9(1)**, 132-136.

[22] AN Usoltsev, IA Shentseva, VR Shayapov, PE Plyusnin, IV korolkov, PA Abramov, MN Sokolov and SA Adonin. Iodide bismuth(iii) complexes with 1-ethyl-3-methylpyridinium: Structure, thermal stability, and optical properties. *Russian Journal of Inorganic Chemistry* 2022; **67**, 1979-1986.

[23] RA Arfah, E Pratiwi, I Raya, H Natsir, P Taba, H Rasyid, M Alfliadhi, AB Khaerunnisa, R Irfandi and S Jarre. Design, synthesis and characterization of Mn(II) cysteine-tyrosine dithiocarbamate complex for against the cancer on MCF-7 breast cancer cell line. *Asian Pacific Journal of Cancer Prevention* 2024; **25(9)**, 3251-3261.

[24] AK Mishra, N Manav and NK Kaushik. Organotin(IV) complexes of thiohydrazones: Synthesis, characterization and antifungal study. *Spectrochimica Acta Part A: Molecular and Biomolecular Spectroscopy* 2005; **61(13-14)**, 3097-3101.

[25] S Santi, AW Wahab, I Raya and A Ahmad. Synthesis and interaction of adenosine-5'-triphosphate with rare earth metal Europium (Eu3+*). AIP Conference Proceedings* 2020; **2296**, 020074.

[26] B Annuar, JO Hill and RJ Magee. Nickel(II) and Copper(II) complexes of mono-ethanol and di-ethanol-dithiocarbamic acid. *Journal of Inorganic and Nuclear Chemistry* 1974; **36(6)**, 1253-1257.

[27] I Sakiyan, R Ozdemir and H Ogutcu. Synthesis, characterization, and antimicrobial activities of new N-(2-hydroxy-1-naphthalidene)-amino acid (L-Tyrosine, L-Arginine, and L-Lysine) Schiff bases and their Manganese (III) complexes. *Synthesis and Reactivity in Inorganic, Metal-Organic, and Nano-Metal Chemistry* 2014; **44(3)**, 417-423.

[28] M Ghorbanloo, M Jaworska, P Paluch, GD Li and L Zhou. Synthesis, characterization, and catalytic activity for thioanisole oxidation of homogeneous and heterogeneous binuclear Manganese(II) complexes with amino acid-based ligands. *Transition Metal Chemistry* 2013; **38**, 511-521.

[29] J Dharmaraja, J Balamurugan and S Shobana. Synthesis, structural elucidation, microbial, antioxidant and nuclease activities of some novel divalent M(II) complexes derived from 5-fluorouracil and l-tyrosine. *Journal of Saudi Chemical Society* 2017; **21(1)**, S67-S76.

[30] S Santi, A Wahab, I Raya, A Ahmad and M Maming. Synthesis, spectroscopic (FT-IR, UV-Visible) study, and homo-lumo analysis of adenosine triphosphate (ATP) doped trivalent terbium. *Journal of Molecular Structure* 2021; **1237**, 130398.

[31] E Pratiwi, I Raya, H Natsir, R Irfandi, P Taba, R Arfah, H Rasyid, Y Hala, S Kasim, AB Khaerunnisa, B Ilham, M Mazaya, Y Tanzil and D

Luthfiana. Investigations of Ni(II)cysteine-tyrosine dithiocarbamate complex: Synthesis, characterization, molecular docking, molecular dynamic, and anticancer activity on MCF-7 breast cancer cell line. *Asian Pacific Journal of Cancer Prevention* 2024; **25(4)**, 1301-1313.

[32] LZ Benet, CM Hosey, O Ursu and TI Oprea. BDDCS, the Rule of 5 and drugability. *Advanced Drug Delivery Reviews* 2016; **101**, 89-98.

[33] CA Lipinski, F Lombardo, BW Dominy and PJ Feeney. experimental and computational approaches to estimate solubility and permeability in drug discovery and development settings. *Advanced Drug Delivery Reviews* 2012; **46(1-3),** 3-26.

[34] J Mosquera, I Garcia and LM Liz-Marzan. Cellular uptake of nanoparticles versus small molecules: A matter of size. *Accounts of Chemical Research* 2018; **51(9)**, 2305-2313.

[35] K Adachi, T Sasaki, A Arai, M Shimizu and H Yamazaki. Impact of variability of *in silico* and *in vitro* octanol/water partition coefficients of compounds on the input parameters and results of simplified human physiologically based pharmacokinetic models after virtual oral administrations. *The Journal of Toxicological Sciences* 2024; **49(10)**, 459-466.

[36] R Raj. Analysis of non-structural proteins, NSPs of SARS-CoV-2 as targets for computational drug designing. *Biochemistry and Biophysics Reports* 2021; **25**, 100847.

[37] I Nyamba, CB Sombie, M Yabre, H Zime-Diawara, J Yameogo, S Ouedraogo, A Lechanteur, R Semde and B Evrard. Pharmaceutical approaches for enhancing solubility and oral bioavailability of poorly soluble drugs. *European Journal of Pharmaceutics and Biopharmaceutics* 2024; **204**, 114513.

[38] EV Radchenko, AS Dyabina, VA Palyulin and NS Zefirov. Prediction of human intestinal absorption of drug compounds. *Russian Chemical Bulletin* 2016; **65**, 576-580.

[39] KMA Azzam. SwissADME and pkCSM webservers predictors: An integrated online platform for accurate and comprehensive predictions for *in silico* ADME/T properties of artemisinin and its derivatives. *Engineering and Technology* 2022; **325(2)**, 14-21.

[40] LM Lagares, Y Perez-Castillo, N Minovski and M Novic. Structure-function relationships in the human p-glycoprotein (abcb1): Insights from molecular dynamics simulations. *International journal of molecular sciences* 2021; **23(1)**, 362.

[41] N Holford and DS Yim. Volume of distribution. *Translational and Clinical Pharmacology* 2016; **24(2)**, 74-77.

[42] JH Lee, S Basith, M Cui, B Kim and S Choi. *In silico* prediction of multiple-category classification model for cytochrome P450 inhibitors and non-inhibitors using machine-learning method. *SAR and QSAR in Environmental Research* 2017; **28(10)**, 863-874.

[43] A Spicakova, P Kraus, T Gucky, V Krystof, M Strnad, V Bazgier, M Otyepka, V Kubickova, M Poruba, Z Racova, I Zapletalova and P Anzenbacher. *In vitro* and *in silico* studies of interaction of synthetic 2,6,9-trisubstituted purine kinase inhibitors BPA-302, BP-21 and BP-117 with liver drug-metabolizing cytochromes P450. *Physiological Research* 2020; **69(4)**, S627-S636.

[44] R Watanabe, R Ohashi, T Esaki, H Kawashima, Y Natsume-Kitatani, C Nagao and K Mizuguchi. Development of an *in silico* prediction system of human renal excretion and clearance from chemical structure information incorporating fraction unbound in plasma as a descriptor. *Scientific Reports* 2019; **9**, 18782.

[45] JC Hancox and AF James. Refining insights into high-affinity drug binding to the human ether-a-go-go-related gene potassium channel. *Molecular pharmacology* 2008; **73(6)**, 1592-1595.

[46] X Duan, X Xiang and J Xie. Crucial components of *Mycobacterium* type II fatty acid biosynthesis (Fas-II) and their inhibitors. *FEMS Microbiology Letters* 2014; **360(2)**, 87-99.

[47] SR Khan, Y Manialawy and AG Siraki. Isoniazid and host immune system interactions: A proposal for a novel comprehensive mode of action. *British Journal of Pharmacology* 2019; **176(24)**, 4599-4608.

[48] MAFA Manan and DB Cordes. Cadmium(II) schiff base complex containing 5-fluoroisatin moiety: Synthesis, characterization, antibacterial

activity and structural studies. *Trends in Sciences* 2022, **19(18)**, 5796.

[49] CI Yeo, ERT Tiekink and J Chew. Insights into the antimicrobial potential of dithiocarbamate anions and metal-based species. *Inorganics* 2021; **9(6)**, 48.